Environ. Sci. Technol. 1991, 25, 1305-1311

Influence of Biofilm Accumulation on Porous Media Hydrodynamics

Alfred B. Cunningham,* William G. Characklis, Feisal Abedeen, and David Crawford

Center for Interfacial Microbial Process Engineering, Montana State University, Bozeman, Montana 59717

■ Laboratory-scale porous media biofilm reactors were used to evaluate the effect of biofilm accumulation, measured as the average thickness along a 50-mm flow path, on media porosity, permeability, and friction factor. Media tested consisted of 1-mm glass spheres, 0.70-mm sand, 0.54-mm sand, and 0.12-mm glass and sand. *Pseudomonas aeruginosa* was used as inoculum and 25 mg L^{-1} glucose substrate was continuously supplied to the reactor. Reactors were operated under constant piezometric head conditions resulting in a flow rate decrease as biofilm developed. The progression of biofilm thickness followed a sigmoidal-shaped curve reaching a maximum thickness after ~5 days. Media porosity decreased between 50 and 96% with increased biofilm accumulation while permeability decreased between 92 and 98%. Porous media friction factor increased substantially for all media tested. Observations of permeability in the biofilm–media matrix indicate that a minimum permeability [(3–7) × 10^{-8} cm^2] persisted after biofilm thickness has reached a maximum value. Such results indicate substantial interaction between mass transport, hydrodynamics, and biofilm accumulation at the fluid–biofilm interface in porous media. Improved understanding of these interactions will lead to industrial and environmental applications in biohydrometallurgy, enhanced oil recovery, and bioremediation of contaminated groundwater and soil.

Introduction

The dynamics of microbial populations in porous media provide significant opportunities for improving the performance of industrial and environmental processes. The mining industry, for example, is developing methods for microbially enhanced leaching of metals from ores and recovery of metals from solutions (*1*). The petroleum industry is likewise interested in controlled biofilm accumulation to aid in enhanced oil recovery operations. Deliberate plugging of high-permeability zones (to prevent injection water from reaching the production well) is valuable (*2, 3*) and can be accomplished by injecting cells and nutrients into the oil-bearing formation. Similarly, controlling biofilm accumulation is important to both injection and production well operation in order to avoid unwanted formation plugging near the well bore. Subsurface biofilms also offer the potential for biotransformation of organic compounds, thereby providing an in situ method (Figure 1) for treating contaminated groundwater supplies (*4–6*). The rate of biotransformation is strongly influenced by porous media mass-transport characteristics including media permeability and pore velocity distribution (*7*), as well as by biofilm surface roughness (*8*) and other variables that affect the delivery rate of substrate and nutrients to growing cells.

Engineering and operational problems associated with these industrial and environmental systems require improved understanding of the interrelationship between porous media hydrodynamic properties and the accumulation rate and spatial distribution of biofilm. This paper presents results of an experimental evaluation of porous media biofilm accumulation and its effects on key hydrodynamic variables including media porosity, permeability, and friction factor.

Biofilm Accumulation. In porous media, as in other aqueous environments, microbial cells may exist in suspension or adsorb firmly to solid surfaces comprising the effective pore space. If favorable environmental conditions persist, adsorbed cells will grow and reproduce at the surface, increasing the amount of attached biomass. Escher (*9*) observed that, under conditions of constant nutrient flux and laminar flow in capillary tubes, sorption-related processes were governed by suspended cell concentration, while the growth process at the surface was a function of microbial surface concentration.

If rates of cell adsorption and growth exceed the rate of desorption, a net accumulation of biomass will result on the surface. As the accumulation process continues, additional cells may attach (and detach) directly to (from) the existing biomass surface. Attachment and detachment are probably the least understood processes affecting the accumulation of biofilm. Trulear and Characklis (*10*) and Chang and Rittman (*11*) used a first-order expression to model net detachment rate (i.e., detachment rate minus attachment rate) as a function of biomass. Speitel and Digiano (*12*) proposed adding a growth-related detachment rate term to the first-order biomass model to account for high detachment rates observed during periods of high cell growth.

Particles of organic and inorganic material flowing in suspension may be removed by the attached biomass through filtration processes including diffusion, interception, and sedimentation (*13*). The entire deposit of cells and polymers, together with captured organic and inorganic particles, is termed the "biofilm". The amount of biofilm accumulation occurring in a porous media flow system is therefore the net result of the biomass added through adsorption, growth, attachment, and filtration less the amount removed by desorption and detachment (Figure 1).

Individual biofilm processes are considerably more difficult to examine in porous media than in other common reactor geometries such as flasks, tanks, reservoirs, and pipelines. Biofilm growth, for example, is complicated by the nature of fluid and nutrient transport which, in porous media, occurs along tortuous flow paths of variable geometry. Similarly, the wide distribution of pore velocities introduces considerable variation in the processes of adsorption, desorption, attachment, and detachment.

Measurement Methods. Recent investigations involving biofilm accumulation in porous media have tended to focus on the increased hydraulic resistance caused by biofilms, rather than direct measurement of accumulation or contributing component processes. Investigations documenting permeability reduction resulting from biofilm accumulation have been reported by practitioners working in petroleum recovery, disposal of treated wastewater, and recharge/recovery operations for water supply (*14–21*). These investigations address a wide variety of porous media, including core samples from field sites as well as synthetic media (e.g., glass spheres). Both pure and mixed bacterial cultures were used as inoculum. Substantial reduction in permeability (65–95%) occurred in all cases. Torbati et al. (*16*) demonstrated that biofilm accumulation preferentially plugged larger pore spaces. Visual obser-

0013-936X/91/0925-1305$02.50/0

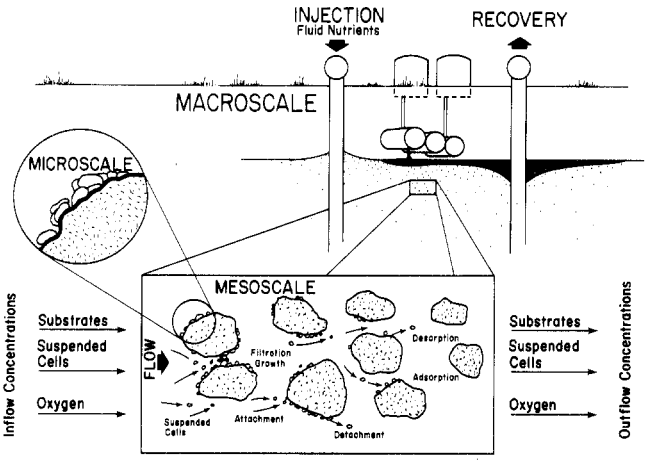

Figure 1. Injection/recovery scheme for enhancing in situ bioremediation of contaminated aquifer. Inset identifies individual microbial transport processes that contribute to biofilm accumulation and activity in porous media.

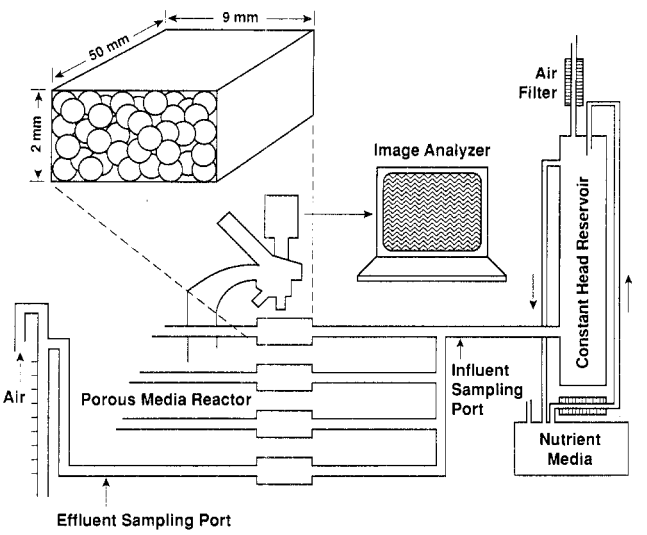

Figure 2. Experimental system for monitoring biofilm accumulation along rectangular porous media reactors.

vation of decreasing microbial mass downstream of the core entrance was reported in several of these investigations.

A computational method for estimating the thickness, L_f, of porous media biofilm was presented by Rittman and McCarty (*22*) as part of a model of steady-state biofilm kinetics. Theoretical biofilm thickness is expressed in terms of substrate flux into the film, specific decay coefficient, average biofilm density, and yield coefficient. Rittman and McCarty also compared computed thickness values with corresponding thickness measurements from a laboratory porous media column reactor. Predicted biofilm thicknesses were found to slightly overestimate corresponding measured values, which were determined on the basis of observed organic carbon content of biofilm attached to individual reactor beads.

As the model of Rittman and McCarty indicates, both thickness and mass density must be measured in order to completely quantify net biofilm accumulation (i.e., the amount of attached biomass per unit surface area). Bakke (*23*) developed an optical method for measuring biofilm thickness and density in situ in capillary tube reactors under laminar flow conditions. The optical thickness observed in these experiments was subsequently corrected by using a geometric analysis of the light path through the sample and the refractive indexes of the sample and surrounding media (*24*). Time progression of biofilm thickness and spatial profiles within the reactor was also obtained by this method, which indicated that film density continued to increase even after the biofilm had reached a quasi-steady-state thickness. Substantial density increase with depth into the biofilm has also been observed (*25*).

In our experiments, average biofilm thickness (measured along the 5-cm reactor) was the variable used to estimate net accumulation. The experimental porous media reactor (Figure 2) allowed optical measurements of biofilm thickness throughout the experiment. Enlarged photographs of media particles showed no detectable difference in biofilm mass density during the 10-day duration of biofilm accumulation. Therefore, the effects of density variation on porous media hydrodynamics were not explicitly evaluated.

Hydrodynamic Variables. The accumulation of biofilm in porous media will result in the reduction in free pore space thereby affecting media hydrodynamic characteristics. Key hydrodynamic variables include the porosity, α, which measures the amount of free pore space, permeability, k, which describes the conductive properties of the media, and friction factor, f, which quantifies frictional resistance. Hydrodynamic equations describing these three variables are summarized in Table I.

Table I. Hydrodynamic Equations Describing Flow in Porous Media

equation	description
$v = -K\,dh/dL$ (1)	Darcy's law
$k = K\nu/g$ (2)	intrinsic permeability
$\alpha = V_p/V_t$ (3)	media porosity
$h_L = \dfrac{f(1-\alpha)Lv^2}{\Theta\alpha^3\,dg}$ (4)	Carmen–Kozeny equation for head loss through porous media
$f = \dfrac{150\,(1-\alpha)+1.75}{N_R}$ (5)	Carmen–Kozeny theoretical equation for factor estimating porous media friction
$N_R = dv/\nu$ (6)	porous media Reynolds number

Terms

variable	description	units
v	specific discharge	mm S^{-1}
K	hydraulic conductivity	mm S^{-1}
k	permeability	cm^2
dh/dL	piezometric gradient	
ν	kinematic viscosity	$m^2\ s^{-1}$
g	gravity constant	9.8 m s^{-2}
α	porosity	
V_P	pore volume in media sample	cm^3
V_T	total volume of media sample	cm^3
h_L	head loss	m
f	porous media friction factor	
d	diameter of media particles	mm
Θ	shape factor (usually 1)	
L	flow path length over which h_L occurs (h_L/L is equal to piezometric gradient)	cm
N_R	porous media Reynolds number	

Materials and Methods

The experimental system (Figure 2) consisted of five parallel, horizontally mounted rectangular porous media reactors. Nutrients were supplied to the reactors under gravity flow from a constant-head mixing chamber. A constant piezometric head drop was maintained across the system throughout each experiment by locating the downstream end of each reactor effluent tube at an ele-

Table II. Composition of Nutrient Solution

constituent	influent concn, g m^{-3}	constituent	influent concn, g m^{-3}
glucose	25.0	$(NH_4)_6MO_7O_{24}\cdot 4H_2O$	0.001
NH_4Cl	7.2	$FeSO_4\cdot 7H_2O$	0.112
$MgSO_4\cdot 7H_2O$	2.0	$ZnSO_4\cdot 7H_2O$	0.10
Na_2HPO_4 (buffer)[a]	213.0	$MnSO_4\cdot H_2O$	0.008
KH_2PO_4 (buffer)[a]	204.5	$CuSO_4\cdot 5H_2O$	0.002
$CaCO_3$	50.0	$Na_2B_4O_7\cdot 10H_2O$	0.001
$(HOCOCH_2)_3N$	0.40		

[a] pH = 6.8.

vation ranging between 2.7 and 16 cm below the level in the constant-head mixing chamber. Flow rate through each reactor varied in proportion to reactor permeability, which decreased substantially during the experiments due to biofilm accumulation. Piezometric head was monitored by vertical standpipe manometers located immediately up- and downstream from the reactor. Flow rate through each reactor was monitored volumetrically by using a graduated pipet located immediately downstream from the reactor.

The thin rectangular geometry of the porous media reactors permitted 10× microscopic observation of biofilm accumulation occurring on porous media particles. Black and white photographs taken through the microscope lens were subsequentually studied by image analysis. The reactors consisted of sand-sized particles encased in rectangular glass capillary tubes of varying thicknesses and 50 mm in length. Both quartz sand and glass spheres were used as media. Median diameters for both sand and glass were 0.12, 0.54, and 1 mm with a coefficient of variation of approximately 15%. Sand (0.70 mm) was also included in the experimental measurement of permeability and porosity. All experiments used layers of media one to three particles in thickness. A light source enhanced the visual image of biofilm accumulation. Media were constrained by fine-mesh wire screen at the reactor ends.

Influent and effluent dissolved oxygen were measured periodically. Because large effluent samples could not be obtained, the Winkler method (*26*) for measuring dissolved oxygen was modified by reducing the volume of samples and all reagents to 10% of their normal amounts. The sodium thiosulfate titrant was likewise reduced from 0.025 to 0.0025 N.

Pseudomonas aeruginosa was used as inoculum in all reactors. The bacteria were cultured aerobically at 20 °C in a batch shake flask containing the nutrient solution described in Table II. *Ps. aeruginosa* was chosen for these experiments because it forms a very uniform biofilm, which facilitates measurement of film thickness on porous media particles. Also, kinetic and stoichiometric coefficients for this organism are well documented (*27*). The entire reactor system was sterilized by autoclaving prior to inoculation. Reactor effluent was checked periodically for contamination by other bacterial species by plate count procedures and subsequent identification of colonies with the API-NFT (Analytab Inc.) procedure.

Biofilm cells were enumerated by removing individual reactor segments and homogenizing in distilled water. Image analysis and epifluorescent staining techniques (*28*) were used to count total cells directly from a sample of homogenized solution. A computer program (*9*) analyzed the raw data and gave the mean cell count from 10 fields of focus on a microscope slide and also gave the standard deviation. Biofilm total organic carbon (TOC) analyses were performed by standard methods using a Dohrmann Model 80 detector. Strong correlation was observed between total cell counts and corresponding TOC measurements (Figure 3).

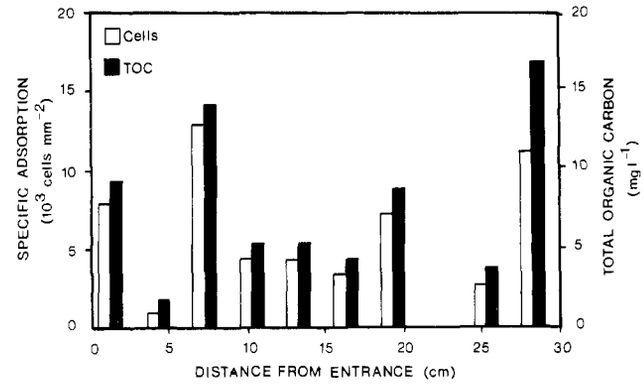

Figure 3. Comparison of cell counts and corresponding TOC measurements for *Ps. aeruginosa* adsorbed to 1-mm glass spheres under no-flow conditions. Measurements were then taken 8 h after inoculation with 5 mL of solution at a concentration of 10^8 cells/mL.

To facilitate the initial adsorption of *Ps. aeruginosa*, 5 mL of concentrated inoculum (approximately 10^8 cells/mL) was injected into each reactor under steady-flow conditions. After an elapsed time equal to the reactor travel time, flow was stopped by clamping both ends of the reactor. After an 8-h period, the reactor was flushed to remove nonadsorbed cells, and a steady-flow condition was established to begin the experiments.

Experimental Results

Biofilm Development. Within 2–3 days after inoculation, a uniform biofilm of detectable thickness could be observed on the exposed edges of reactor media particles. Average biofilm thickness (L_f) measurements were taken based on 8–10 thicknesses taken at equal intervals along the reactor (coefficient of variation of 10–15%). No obvious difference in biofilm thickness was detected between the upstream and downstream ends of the 5-cm reactors. Photographs of reactor contents (*6*) permitted more detailed examination of biomass distribution. Two days after inoculation, a biofilm of approximately 15-μm thickness had developed on the visible edges of the 1-mm glass spheres. After ~5 days, "pockets" of accumulation appeared approximately 50 μm in radius located on the downstream side of the contact points between particles. These locations appeared to be relatively sheltered from shear stress compared to surfaces located away from points of contact. After 8 days, biofilm thickness had increased to ~60 μm and had displaced a substantial part of the original pore space inside the 1-mm glass spheres reactor. Similar progressions were observed for the other types of porous media.

The progression of biofilm thickness for porous media of various size and composition was generated by simultaneously running five parallel reactors under a constant piezometric head gradient of 0.5 cm/cm (Figure 4). Comparison of these accumulation curves indicates that the ultimate biofilm thickness varied directly with media pore space size and was not influenced significantly by media composition. A similar observation was made with "empty" rectangular reactors (i.e., containing no porous media) of dimensions 0.2 × 4 mm on 0.4 × 4 mm; the reactor with the larger cross section (0.4 × 4 mm) and, hence the larger mass flux, exhibited a greater maximum biofilm thickness.

Permeability Reduction. A constant piezometric gradient was maintained across each porous media reactor throughout the experiment and flow rates were measured

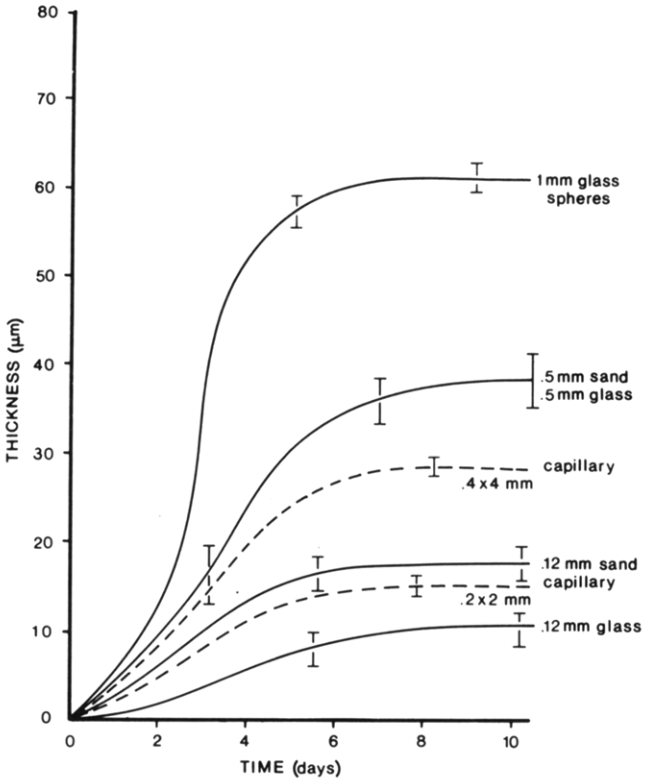

Figure 4. Progression of biofilm thickness (*Ps. aeruginosa*) for media of different diameter and composition. All reactors were run in parallel under a piezometric gradient of 0.5.

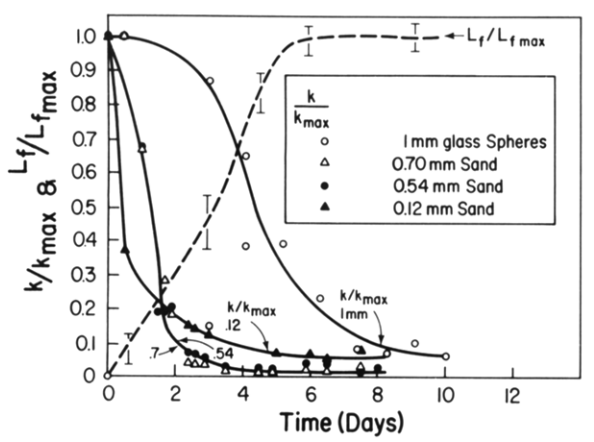

Figure 5. Porous media permeability decrease corresponding to increased biofilm thickness. $L_f/L_{f\,max}$ is a single composite dimensionless curve representing all thickness curves from Figure 4. K_{max} values are 2.1×10^{-5} (1-mm glass spheres), 3.19×10^{-6} (0.70-mm sand), 2.17×10^{-6} (0.54-mm sand), and 9.7×10^{-7} cm^2 (0.12-mm sand).

volumetrically at 12-h intervals. From these data, together with reactor geometry, permeability values were computed from eqs 1 and 2. Initial (clean surface) permeability values were 2.1×10^{-5} (1-mm glass spheres), 3.19×10^{-6} (0.70-mm sand), 2.17×10^{-6} (0.54-mm sand), and 9.7×10^{-7} cm^2 (0.12-mm sand). Increases in average biofilm thickness in the 5-cm porous media reactors resulted in a corresponding decrease in permeability (Figure 5). In each experiment, the permeability decreased rapidly during the period of increasing biofilm thickness and then stabilized in the range between 1 and 5% of the original (clean surface) value. Also, the permeability for 0.7-, 0.54-, and 0.12-mm sand all achieved a relatively stable minimum permeability between about 3×10^{-8} and 7×10^{-8} cm^2.

Porosity Effects. The accumulation of biofilm in porous media resulted in a corresponding decrease in media

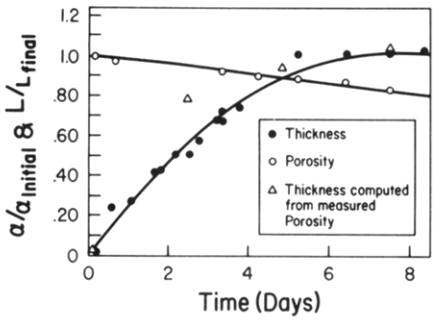

Figure 6. Effective porosity (determined by using bromothymol blue dye tracer) compared with optical measurements of average biofilm thickness computed (using eq 8) for effective porosities of 0.42, 0.40, 0.38, and 0.36. $L_{final} = 25$ μm and $\alpha_{initial} = 0.42$.

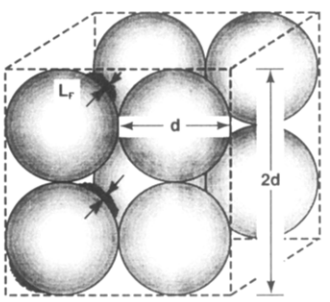

Figure 7. Cubic packing of uniform diameter spherical porous media. L_f is average biofilm thickness measured on media surface.

porosity (Figure 6). Initial media porosity (0.42) was measured by oven-drying the saturated reactor media. Subsequent porosity values with the biofilm in place were estimated as

$$\alpha = v/v_p \tag{7}$$

where v_p is the average linear pore velocity through the porous media, v is the specific discharge (flow rate/cross-sectional area) for the reactor, and α is the effective porosity. Measurements of v were determined volumetrically, while corresponding measurements of v_p were made using bromothymol blue dye tracer monitored with a pair of infrared light sensors mounted at either end of the reactor.

Tests on each medium type (prior to biofilm development) resulted in no significant difference between total porosity, as determined by oven-drying, and effective porosity determined by dye tracer measurement of v_p. Comparable tests could not be run with biofilm in place because oven-drying would destroy the biofilm.

In these experiments, biofilm thickness L_f was calculated from observations for α at various stages of biofilm development. If biofilm is assumed uniformly distributed over media particles, an estimate of biofilm thickness can be made as follows:

$$L_f = V_f/S \tag{8}$$

where V_f is the biofilm volume, determined as the difference between V_p values (using eq 3) measured before and after biofilm accumulation, and S is the total surface area inside the porous media reactor.

The measured α values (Figure 6), together with eq 3, were used to compute corresponding biofilm thicknesses (Δ in Figure 6) from eq 8. The computed L_f values (corresponding to α values of 0.42, 0.40, 0.38, and 0.36) compare favorably with corresponding microscopic measurements of average thickness. This observation points out the potential for developing methods for estimating biofilm accumulation in a porous media sample based on dye

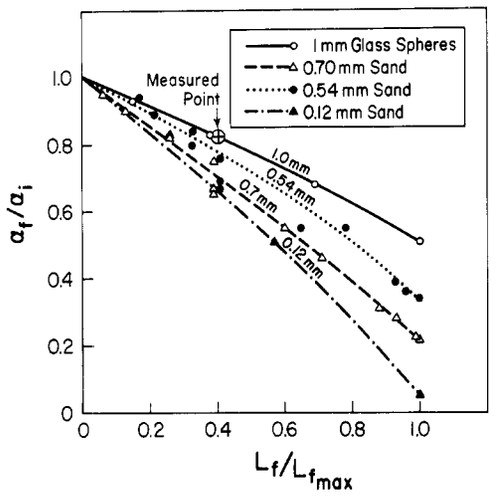

Figure 8. Variation in estimated media porosity, α_f with biofilm thickness. For 1-mm glass spheres $\alpha_{max} = 0.48$, $L_{f\,max} = 65$ μm; for 0.7-mm sand $\alpha_{max} = 0.35$, $L_{f\,max} = 15.4$ μm; for 0.54-mm sand $\alpha_{max} = 0.35$, $L_{f\,max} = 46$ μm; for 0.12-mm sand $\alpha_{max} = 0.47$, $L_{f\,max} = 15.3$ μm. The ⊕ symbol represents measured α_f (0.34) and L_f (25 μm) for 1-mm glass spheres.

tracer measurements of effective porosity. Such nondestructive methods could be particularly useful in the analysis of field core samples.

Theoretical Porosity. The concept of theoretical porosity (*29*), which assumes uniform diameter spherical porous media particles arranged as in Figure 7, can be used here to develop an expression relating effective porosity and biofilm thickness. If effects of biofilm are considered the expression for theoretical porosity, α_{tf} is

$$\alpha_{tf} = \frac{V_p}{V_T} = \frac{4d^3 - 4(\pi/6)(d + 2L_f)^3}{4d^3}$$

or

$$\alpha_{tf} = 1 - \frac{(\pi/6)(d + 2L_f)^3}{d^3} \qquad (9)$$

(for the clean surface conditions ($L_f = 0$), α_{tf} can be calculated as 0.476).

Biofilm Porosity Estimates. Equation 9, along with clean surface porosity measurements, was used to estimate effective porosity variation with biofilm development for each experimental porous medium. Media porosity with biofilm, α_f, was computed by using the proportionality relationship

$$\alpha_f/\alpha_i = \alpha_{tf}/0.476 \qquad (10)$$

where α_{tf} was computed (eq 9) for each measured value of L_f, 0.476 was the theoretical clean surface porosity, and α_i was the measured clean surface porosity. Estimates of α_f using eq 10 appear in Figure 8. A measured α_f value of 0.34 was determined from eq 7 (v_p measured via bromothymol blue dye tracer) for 1-mm glass spheres with an L_f of 25 μm. These measurements agree favorably with the corresponding α_f estimated from eq 10 (⊕ symbol in Figure 8).

Porous Media Friction Factor. Reactor flow rate and piezometric gradient measurements, together with the porosity values (Figure 8), were also used to compute porous media friction factor (eq 4). Comparisons were made between measured f and corresponding values computed from Kozeny–Carmen's theoretical relationship (eqs 5 and 6), which predicts f in terms of porous media Reynolds number, N_r (Figure 9). The degree and symmetry of point scatter in Figure 9 provides a general indication of the

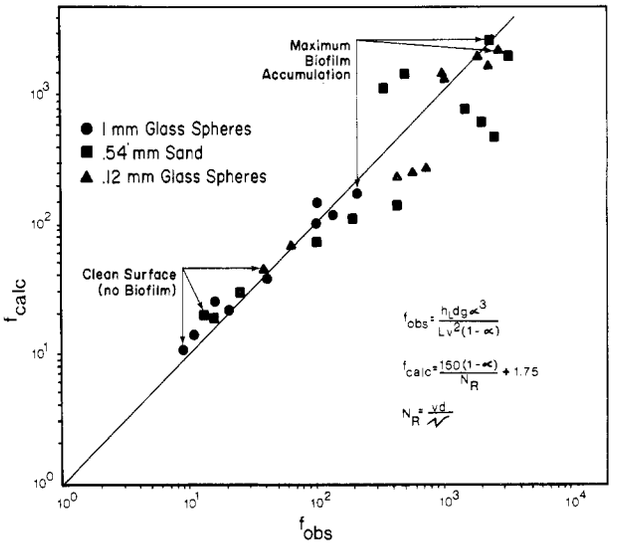

Figure 9. Comparison of measured porous media friction factors with values computed by using the Carmen–Kozeny equation (eq 5).

validity of using eq 10 to estimate effective porosity for biofilm-laden porous media. Predicted and measured f values were found to agree well (Figure 9) during early stages of biofilm development when the reactor flow regime was in the transitional region between turbulent and laminar flow. Increased scatter occurring for the higher f values is probably the result of decreased accuracy in measuring the (very low) flow rates resulting from larger biofilm thicknesses. Friction factor increased substantially with increasing biofilm thickness for all types of media tested. Smaller diameter media resulted in higher f values for the condition of maximum biofilm thickness.

Discussion

In our experiments, *Ps. aeruginosa* inoculum was injected, along with nutrients necessary for cell growth, into initially sterile porous media. Under these conditions, some cells will adsorb to the media particles, consume substrate, and grow. Many cells desorb back into suspension. According to Escher (*9*), rates of adsorption and desorption depend on suspended cell concentration and the magnitude of shear stress at the substratum. If sufficient substrate and nutrients are available, the colonies will grow together to form a continuous film. If pore sizes (with or without biofilm) are small enough, biofilm accumulation will be enhanced by the process of filtration. The presence of significant surface irregularities on the biofilm will most likely increase filtration potential. As the biofilm continues to develop, suspended cells will attach to and detach from the biofilm surface.

As biofilm thickness increases, the diffusional path length within the biofilm increases thereby decreasing nutrient concentrations in the base film. Providing the piezometric head gradient remains constant, increased thickness will also result in decreased pore velocity. Decreased pore velocities will reduce both advective and dispersive transport thereby lowering nutrient concentrations at the film–water interface, which will subsequently reduce growth rate. Decreased pore velocities will also reduce shear stress, thereby reducing the rate of detachment. Accumulation of biofilm will continue until specific growth rate is balanced by detachment rate. These interactions give rise to the sigmoidal shape exhibited by the accumulation progressions (Figure 4), which indicate a quasi-steady-state thickness is reached after ~5 days of reactor operation. Maximum biofilm thickness values of

63, 40, and 9–14 μm were observed (Figure 4) for media particle diameters of 1, 0.54, and 0.12 mm. Clean surface permeability values of 2.1×10^{-5}, 2.17×10^{-6}, and 9.7×10^{-7} cm^2 correspond to these particle diameters, suggesting a direct relationship between media permeability and maximum biofilm thickness.

After biofilm thickness reaches quasi steady state, the volume of effective pore space (permeability) appears to stabilize and remain constant until operating conditions are disturbed. The media/biofilm permeability (for media of various size and composition) stabilized and remained essentially constant after ~5 days of reactor operation (Figure 5). Torbati et al. (*16*) reported a similar observation wherein in situ accumulation of microorganisms in Berea sandstone was observed to preferentially plus the large (59–69 μm) pore entrances resulting in a narrow range of biofilm-encased pore sizes in the range of 5–30 μm. These observations suggest that, for the experimental conditions used herein, the biofilm accumulation process stabilizes so as to preserve a minimum permeability within the media biofilm matrix.

If sufficient biomass accumulates so as to reduce the effective pore space, a corresponding decrease in media porosity and permeability, as well as an increase in friction factor will ensue (Figures 5, 8, and 9). The strong correlation observed between these three variables and biofilm thickness is important because it provides the basis for developing potentially useful predictive relationships. For example, if biofilm thickness can be measured or computed based on kinetic parameters (*22*), estimates of corresponding k, α, and f can be made from curve relationships illustrated in Figures 5–9. Conversely, if in situ measurements of effective porosity can be made, estimates of biofilm thickness can be computed from eq 8.

Conclusions

Our experiments have related porous media biofilm thickness with media porosity, permeability, and friction factor under the following conditions: a *Ps. aeruginosa* biofilm developed within uniform diameter porous media reactors, operated under a constant piezometric gradient, with a sterile influent. With these experimental conditions in mind, the following conclusions can be drawn:

(1) The maximum biofilm thickness varied directly with the initial (clean surface) permeability of the media. Biofilm accumulation followed the same sigmoidal-shaped progression observed in conduit reactor systems.

(2) When biofilm accumulation becomes large enough to substantially reduce pore space, media permeability and porosity will decrease substantially and friction factor will increase substantially.

(3) As the accumulation process progressed in our experiments, the permeability of the biofilm–media matrix stabilized at a minimum value [$(3–7) \times 10^{-8}$ cm^2] regardless of media particle diameter.

(4) Predictions of formation plugging and biofilm accumulation in porous media can be accomplished based on biofilm kinetics and the concept of theoretical porosity.

Acknowledgments

We acknowledge the assistance of Anne Camper, Research Associate of the Center for Interfacial Microbial Process Engineering, Montana State University, in experimental design and microbial analyses. Dr. Edward Bouwer of the Department of Geography and Environmental Engineering, The Johns Hopkins University, provided insight and manuscript review.

Literature Cited

(1) Ehrlich, H. L.; Holms, D. S. Workshop proceedings, Rensselaer Polytechnic Institute, Troy, NY, May 28–30, 1985.
(2) Raiders, R. A.; Knapp, R. M.; McInerney, M. J. *J. Ind. Microbiol.* **1989**, *4*, 215–230.
(3) MacLeod, F. A.; Lappin-Scott, H. M.; Costerton, J. W. *Appl. Environ. Microbiol.* **1988**, *54*, 1365–1372.
(4) Wilson, B. H.; Smith, G. B.; Rees, J. F. *Environ. Sci. Technol.* **1986**, *20*, 997–1002.
(5) Bouwer, E. J.; McCarty, P. L.; Bouwer, H.; Rice, R. C. *Water. Res.* **1984**, *18*, 463–472.
(6) Cunningham, A. B.; Bouwer, E. J.; Characklis, W. G. *Biofilms*; Characklis, W. G., Marshall, K. C., Eds.; New York, 1990; Chapter 18, pp 697–732.
(7) Novac, J. T.; Hickman, G. T.; Morris, M. A.; Benoit, R. E. Bulletin 165; Virginia Water Resources Research Center, Virginia Polytechnic Institute and State University, Blacksburg, VA, 1989.
(8) Siegrist, H.; Gujer, W. *Water Res.* **1985**, *19*, 1369–1378.
(9) Escher, A. R. Ph.D. Dissertation, Dept. of Civil Engineering/Engineering Mechanics, Bozeman MT, 1986; pp 37–38.
(10) Trulear, M. G.; Characklis, W. G. *J.—Water Pollut. Control Fed.* **1982**, *54*, 1288–1301.
(11) Chang, H. T.; Rittman, B. E. *J.—Water Pollut. Control Fed.* **1988**, *60*, 362–368.
(12) Speitel, G. E., Jr.; Digiano, F. A. *J. Environ. Eng.* **1987**, *113*, 464–475.
(13) Bouwer, E. J. *Water Res.* **1987**, *21*, 1489–1498.
(14) Shaw, J. C.; Bramhill, B.; Wardlaw, N. C.; Costerton, J. W. *Appl. Environ. Microbiol.* **1985**, *49*, 693–701.
(15) Raiders, R. A.; McInerney, M. J.; Revus, D. E.; Torbati, H. M.; Knapp, R. M.; Jenneman, G. E. *J. Ind. Microbiol.* **1986**, *1*, 195–203.
(16) Torbati, H. M.; Raiders, R. A.; Donaldson, E. C.; McInerney, M. J.; Jenneman, G. E.; Knapp, R. M. *J. Ind. Microbiol.* **1986**, *1*, 227–234.
(17) Raleigh, J. T.; Flock, D. L. *Pet. Trans., Pet Nat. Gas. Div.* **1965**, *68*, 201–206.
(18) Hart, R. T.; Fekete, T.; Flock, D. L. *Can. Min. Metall. Bull.* **1960**, *63*, 495–501.
(19) Cerini, W. G.; Battles, W. R.; Jones, P. H. *Pet. Technol.* **1946**, *9*, 2028.
(20) Jenneman, G. E.; McInerney, M. J.; Knapp, R. M. *Appl. Environ. Microbiol.* **1985**, *50*, 383–391.
(21) Okubo, T.; Matsumoto, J. *Water Res.* **1983**, *17*, 813–821.
(22) Rittman, B. E.; McCarty, P. L. *Biotechnol. Bioeng.* **1980**, *22*, 2343–2357.
(23) Bakke, R. Ph.D. Dissertation, Dept. of Civil Engineering/Engineering Mechanics, Montana State University, Bozeman, MT, 1986.
(24) Bakke, R.; Olsson, P. W. *J. Microbiol. Methods* **1986**, *5*, 93–98.
(25) Characklis, W. G.; Marshall, K. C. *Biofilms*; John Wiley & Sons: New York, 1990; pp 110–112.
(26) *Standard Methods for the Examination of Water and Wastewater*, 13th ed.; American Public Health Association: Washington, DC, 1979.
(27) Bakke, R.; Trulear, M. G.; Characklis, W. G. *Biotechnol. Bioeng.* **1984**, *26*, 1418–1424.
(28) Hobbie, J. E.; Daley, R. J.; Jasper, S. *Appl. Environ. Microbiol.* **1977**, *33*, 1225–1228.
(29) Bouwer, H. *Groundwater Hydrology*; McGraw-Hill: New York, 1978; p 21.

Received for review August 27, 1990. Revised manuscript received January 29, 1991. Accepted January 29, 1991. We acknowledge support from the Center for Interfacial Microbial Process Engineering at Montana State University, a National Science Foundation Engineering Research Center and the Center's Industrial Associates. Although the research described in this

article has been funded in part by the U.S. Environmental Protection Agency under Assistance Agreement R-815709 to Montana State University through the Hazardous Substance Research Center for U.S. EPA regions 7 and 8 headquartered at Kansas State University, it has not been subjected to the Agency's peer and administrative review and, therefore, may not necessarily reflect the views of the Agency, and no official endorsement should be inferred. This research was also supported by the U.S. Geological Survey (Project 14-08-0001-G1284).

Quantitative Characterization of Urban Sources of Organic Aerosol by High-Resolution Gas Chromatography

Lynn M. Hildemann,† Monica A. Mazurek,‡ and Glen R. Cass*

Environmental Engineering Science Department and Environmental Quality Laboratory, California Institute of Technology, Pasadena, California 91125

Bernd R. T. Simoneit

College of Oceanography, Oregon State University, Corvallis, Oregon 97331

■ Fine aerosol emissions have been collected from a variety of urban combustion sources, including an industrial boiler, a fireplace, automobiles, diesel trucks, gas-fired home appliances, and meat cooking operations, by use of a dilution sampling system. Other sampling techniques have been utilized to collect fine aerosol samples of paved road dust, brake wear, tire wear, cigarette smoke, tar pot emissions, and vegetative detritus. The organic matter contained in each of these samples has been analyzed via high-resolution gas chromatography. By use of a simple computational approach, a quantitative, 50-parameter characterization of the elutable fine organic aerosol emitted from each source type has been determined. The organic mass distribution fingerprints obtained by this approach are shown to differ significantly from each other for most of the source types tested, using hierarchical cluster analysis.

Introduction

Most of the existing data on organic aerosol emissions from sources are derived from bulk chemical analyses that quantify the total amount of organic carbon present. Total aerosol emissions of organic carbon have been measured by combustion techniques for a large variety of sources (e.g., refs 1 and 2). Gravimetric procedures have been used to quantify the amount of extractable organic material emitted from sources such as boilers (e.g., refs 3–5), motor vehicles (e.g., refs 6–9), and fireplaces (e.g., refs 10 and 11). Some separation of the organic species based on vaporization temperature also has been achieved by using thermal evolution analysis to produce "thermograms" (*12–17*). These approaches provide little or no information about the underlying molecular structure of the organic aerosol compounds emitted.

Other researchers have used costly, time-consuming procedures to identify specific organic compounds (e.g., polycyclic aromatic hydrocarbons) through approaches such as gas chromatography coupled with mass spectrometry (GC/MS) and high-pressure liquid chromatography with fluorescence detection. Daisey and co-workers (*18*) have published a thorough review of the literature between 1972 and 1986 that identifies specific organic compounds in various source emissions. The individual compounds identified typically account for only a few percent of the total organic mass emitted. Hence these data are of limited use in designing pollution abatement programs that must achieve changes in the total amount of aerosol present.

Aerosol carbon emissions arise from a large number of different source types. Recent studies of Los Angeles (*19, 20*) have shown that at least a dozen different source types must be considered in order to account for close to 80% of the primary organic aerosol emissions in that airshed. To determine the effect of these emission sources on ambient air quality via receptor modeling techniques, at the very least there must be more distinctive attributes of the organic aerosol than there are different source types. The predictions of transport-oriented models in relating source contributions to the ambient organic aerosol likewise require detailed characterization of the emission sources for model verification. In both air quality modeling approaches, a procedure is needed for characterizing the organic aerosol emission sources that is more economical than GC/MS analysis, but provides a fuller description of the differences between the source types than is possible from bulk carbon analysis.

In the present study, gas chromatography (GC) analyses alone are used to characterize the organic aerosol emissions from a variety of sources in a way that reveals the distinctive features of the different source types using a quantitative, multiparameter description. This approach shows promise as a tool for characterizing organic emissions in a way that can be used to better support air quality modeling studies.

Experimental Section

Sample Collection. Fine organic aerosol (particle diameter $d_p < 2$ μm) was collected from combustion sources by a dilution stack sampling system, and other sources were sampled by grab sampling techniques. The source types tested and the number of samples analyzed are itemized in Table I. Details of the sampling procedures used for each of the sources have been described elsewhere (*19*), and the design of the stack sampler has been documented previously (*21*).

Briefly, hot stack gases were diluted many-fold with purified dilution air that had passed through an activated carbon bed and an absolute filter. During the dilution process, the source effluent was cooled to ambient temperature and kept at near-ambient pressure, causing the aerosol-forming organic vapors present to condense onto preexisting aerosol as would normally occur in the plume downwind of the stack. The diluted emissions passed through a 2-μm size-cut cyclone, and the fine particulate

† Present address: Department of Civil Engineering, Stanford University, Stanford, CA 94305-4020.

‡ Present address: Environmental Chemistry Division, Bldg. 426, Brookhaven National Laboratory, Upton, NY 11973.

0013-936X/91/0925-1311$02.50/0